

# Possibilities of the X-ray diffraction data processing method for detecting reflections with intensity below the background noise component

S.V. Gabelkov <sup>a)</sup> I.V. Zhyganiuk , A.D. Skorbut, V.G. Kudlai , B.S. Savchenko, P.E. Parkhomchuk, and S.O. Chikolovets 

*Institute for Safety Problems of Nuclear Power Plants, National Academy of Sciences of Ukraine, st. Kirova 36a, Chornobyl 07270, Ukraine*

(Received 7 September 2023; accepted 5 May 2024)

The values of the signal-to-noise ratio are determined, at which the method of processing X-ray diffraction data reveals reflections with intensity less than the noise component of the background. The possibilities of the method are demonstrated on weak reflections of  $\alpha$ -quartz. The method of processing X-ray diffraction data makes it possible to increase the possibilities of X-ray phase analysis in determining the qualitative phase composition of multiphase materials with a small (down to 0.1 wt.%) content of several (up to eight) phases.

© The Author(s), 2024. Published by Cambridge University Press on behalf of International Centre for Diffraction Data. This is an Open Access article, distributed under the terms of the Creative Commons Attribution licence (<http://creativecommons.org/licenses/by/4.0/>), which permits unrestricted re-use, distribution and reproduction, provided the original article is properly cited.

[doi:10.1017/S0885715624000241]

Keywords: x-ray phase analysis, crystalline phases, diffraction reflections, signal-to-noise ratio, permutation test, lava-like fuel-containing materials (LFCM)

## I. INTRODUCTION

The method of X-ray phase analysis is widely used to study many types of materials (steels (Garin and Mannheim, 2012), alloys (Sariel et al., 2008), glass ceramics (Wilkins et al., 2020; Loy et al., 2017), ceramics (Murugesan et al., 2023), etc.) containing crystalline phases. The vast majority of researchers usually use a very high signal-to-noise ratio when registering reflections. The number of measured impulses is often in the range of hundreds of thousands for intense peaks and cannot be below tens of thousands for secondary peaks (Guinebretière, 2007). However, in practice, the signal-to-noise ratio may not have large values, for example, 80–130 (Garin and Mannheim, 2012), ~70 (Sariel et al., 2008), 30–60 (Wilkins et al., 2020), and ~45 (Loy et al., 2017).

The symbol list below defines the symbols used in this manuscript.

Symbol list:

$I$  is the normalized intensity of reflection of the crystalline phase on the diffraction pattern;

$2\theta$  is the angle location of the crystalline phase reflection on the diffraction pattern;

$d$  is the interplanar distance;

$t$  is the counting time;

$I_b$  is the intensity value at the  $2\theta$  angle of the diffraction pattern obtained without a specimen (diffractometer background intensity value);

$I_{b-\max}$  is the maximum background intensity;

$I_{b-\min}$  is the minimum background intensity;

$(I_{b-\max} - I_{b-\min})$  is the difference between the maximum and minimum values of the diffractometer background intensities;

$\langle I_b \rangle$  is the average diffractometer background intensity in the  $[\theta_1, \theta_2]$  angle range;

$\sigma_b$  is the rms deviation of the average value of the diffractometer background intensity in the angle range of  $[\theta_1, \theta_2]$ ;

$\Delta I_b$  is the “noise” component of the diffractometer background intensity in the  $[\theta_1, \theta_2]$  angle range;

$I_b^c$  is the maximum intensity of pseudo-reflections on the correlation pattern after applying the data processing method to the intensity values of the diffractometer background in the  $[\theta_1, \theta_2]$  angle range;

$2\theta_b^c$  is the angle corresponding to the pseudo-reflection on the correlation pattern;

$I_q^d$  is the  $\alpha$ -quartz reflection intensity on the diffraction pattern;

$2\theta_q^d$  is the angle of the  $\alpha$ -quartz reflection;

$\beta$  is the FWHM;

$I_q^c$  is the reflection intensity of  $\alpha$ -quartz on the correlation pattern after applying the data processing method;

$2\theta_q^c$  is the angle of the  $\alpha$ -quartz reflection on the correlation pattern after applying the data processing method;

$\langle I_q^d \rangle$  is the average value of  $\alpha$ -quartz reflection intensity;

$\langle I_q^c \rangle$  is the average intensity of  $\alpha$ -quartz reflection on the correlation pattern after applying the data processing method;

$I_q^d/\Delta I_b$  is the ratio of the  $\alpha$ -quartz reflection intensity to the value of the “noise” component of the diffractometer background intensity on the diffraction pattern (signal-to-noise ratio).

$\{2\theta_i; I_i\}$ ,  $i = 1 \dots n$ ,  $n \in \mathbb{Z}^+$  is the array of obtained experimental data (angles and intensities);

<sup>a)</sup> Author to whom correspondence should be addressed. Electronic mail: [s.gabelkov@isnpp.kiev.ua](mailto:s.gabelkov@isnpp.kiev.ua)



$I^{(\text{expr})} = \{2\theta_{m+1}^{(\text{expr})} \dots 2\theta_{m+k}^{(\text{expr})}; I_{m+1}^{(\text{expr})} \dots I_{m+k}^{(\text{expr})}\}$  is a limited sample from an array of experimental data in the range of angles from  $2\theta_{m+1}^{(\text{expr})}$  to  $2\theta_{m+k}^{(\text{expr})}$ ;  
 $I^{(\text{mod})} = \{2\theta_1^{(\text{mod})} \dots 2\theta_k^{(\text{mod})}; I_1^{(\text{mod})} \dots I_k^{(\text{mod})}\}$  is a model data sampling in the range of angles from  $2\theta_1^{(\text{mod})}$  to  $2\theta_k^{(\text{mod})}$ ;  
 $S_0$  is the initial correlation degree between the model and experimental data samples;  
 $I_r^{(\text{prm})}$  are intensity values from the experimental sample  $I^{(\text{expr})}$  after permutation of two intensity values;  
 $\pi$  is the permutation function;  
 $S_{\text{prm } j}$  is the current value of the correlation degree;  
 $L_j$  is a numerical value of the difference between the current and initial values of the correlation degree  $L_j = |S_{\text{prm } j} - S_0|$ ;  
 $L_{\text{max}}$  is the maximum  $L_j$  value in the presence of a local maximum on the histogram;  
 $I_i^c$  is an intensity on the correlation pattern in accordance with formula (4);  
 $\{2\theta_i; I_i^c\}$ ,  $i = 1 \dots n$ ,  $n \in \mathbb{Z}^+$  is an array of correlation data obtained as a result of applying our method of processing X-ray diffraction data;

*Explanations on symbol indices.* Symbols with index  $b$  refer to the background;  $q$  refers to  $\alpha$ -quartz reflections;  $d$  refers to reflections on the diffraction pattern;  $c$  refers to reflections on the correlation pattern.

*Comments to the symbol list:*  $I_b, I_q^d, 2\theta_q^d$  are observed diffraction data;  $I_b^c, 2\theta_b^c, I_q^c, 2\theta_q^c$  are calculated diffraction data:

However, situations are possible when researchers are forced to be satisfied with a low signal-to-noise ratio (values 3–4 (Loy et al., 2017)). This, for example, occurs if the time of studying the sample is limited when determining the phase composition and the content of the detected phases of steel directly in the process of its heat treatment (Wiessner et al., 2021). In that study, the recording time of one diffraction pattern is limited to 700 s. The signal-to-noise ratio was in the range from 7 to 1.5.

The same situation is possible when researchers are dealing with a multiphase material and where the content of several phases is low (down to 0.1 wt.%). The recording time of one diffraction pattern has to be increased not only to obtain reliable data on the reflection with low intensity but also due to a significant number of these reflections (possibly 10–20 reflections from 3 to 5 crystalline phases). For example, the authors studied lava-like fuel-containing materials (LFCM) (black ceramics) obtained as a result of the accident at the fourth unit of the Chernobyl nuclear power plant (Gabelkov et al., 2023). It was possible to obtain data on 78 reflections, 76 of which were identified from noise using the herein-described method. From these reflections, nine phases were identified. The signal-to-noise ratio was in the range from 4 to 0.3.

The signal-to-noise ratio can be improved for part of the diffraction pattern angular ranges. We can use the concept of a variable-counting time (VCT) strategy (Madsen and Hill, 1994). This strategy is based on a function that increases the counting time used at each step in the scan in a manner that is inversely proportional to the decline in reflection intensity. This concept optimizes the acquisition time of diffraction data. However, it is not effective in the case of a large number of reflections with low intensity, i.e. for multiphase materials with a low content of the studied phases. You have to either increase the time it takes to obtain a diffraction pattern to

unrealistic intervals or work with reflections that have a low signal-to-noise ratio.

In the practice of X-ray phase analysis, in most cases, we are dealing with materials that contain one, two, and much less often three main crystalline phases, with the possible presence of several more phases in an amount of not more than a few percent (most often tenths of a percent or less). Data on phase composition and content of crystalline phases in small quantities can improve the characteristics of materials, and their parameters of preparation and use. The presence of crystalline phases with a low content in the material may be due to the presence of unavoidable impurities and/or specially introduced additives. Unfortunately, there can be several such phases (two, three, or more) and their influence on the characteristics of the material is different. Some of them are useful, for example, they improve the characteristics of the material and simplify or reduce the cost of technology. The presence of others worsens the characteristics of the material. The influence of some of them has not yet been established.

To obtain more complete information about the phase composition of the material, it is desirable to identify crystalline phases with a low content and evaluate them. To do this, you can increase the recording time of the diffraction pattern or use a sensitive detector with low noise on the diffractometer, which increases the time or cost of research equipment. It is much more efficient to apply data processing methods, for example, our X-ray diffraction data processing method for multiphase materials with a low content of phases (Skorbun et al., 2019).

The purpose of this work is to determine the possibilities of the X-ray diffraction data processing method for multiphase materials with low-phase contents to identify weak reflections of crystalline phases with an intensity less than the background noise component.

## II. EXPERIMENTAL

### A. Research materials

The study used a specimen of  $\alpha$ -quartz powder placed in a cuvette. A specimen of brown LFCM ceramics, typical for room 304/2 and the steam distribution corridor of the fourth block of the Chernobyl nuclear power plant, was placed under the cuvette. The specimen of  $\alpha$ -quartz powder was chosen to determine the possibilities of our diffraction data processing method.  $\alpha$ -quartz is a stable phase of silicon oxide and has been well studied. The specimen of LFCM brown ceramics was used to increase the background values in the diffraction pattern.

### B. X-ray diffraction measurement

Data on  $\alpha$ -quartz reflections were obtained on a modernized DRON-4 diffractometer, scheme  $\theta$ – $2\theta$ , Cu  $K\alpha$  radiation (30 kV, 20 mA), monochromator – graphite single crystal. The step size was  $0.05^\circ$ . The counting times per point were 65, 195, and 390 s (“large” counting time) and from 5 to 60 s in increments of 5 s (“small” counting time). A screen was put in place to reduce the effect of  $\gamma$ -radiation from the studied specimens on the useful signal recording system. Additional protective barriers were using to protect personnel from  $\gamma$ -radiation of LFCM.

### C. X-ray diffraction data processing method

X-ray diffraction data were processed by a fundamentally new method of correlation analysis using computational statistics (Skorbun et al., 2019). This method was specifically created for processing X-ray diffraction data from low-content multiphase materials. The method uses the permutation test, the Monte Carlo method, and other computer statistics methods (Moore et al. 2014).

We create an array of experimental data  $\{2\theta_i; I_i\}$  from the corresponding values of angles and intensities. Next, we take part of this array for the values  $i = m \dots m+k$ ;  $m, k \in \mathbb{Z}^+$ . This part of the data array may contain one reflection with a FWHM equal to the experimental width ( $\beta$ ) of the reflection.

Subsequently, the correlation value between the limited sample is calculated:  $I^{(\text{expr})} = \{2\theta_{m+1}^{(\text{expr})} \dots 2\theta_{m+k}^{(\text{expr})}; I_{m+1}^{(\text{expr})} \dots I_{m+k}^{(\text{expr})}\}$  from an array of experimental data with a model data sample  $I^{(\text{mod})} = \{2\theta_1^{(\text{mod})} \dots 2\theta_k^{(\text{mod})}; I_1^{(\text{mod})} \dots I_k^{(\text{mod})}\}$ , which models one reflection. The model sample  $I^{(\text{mod})}$  is formed in the angle range from  $2\theta_1^{(\text{mod})}$  to  $2\theta_k^{(\text{mod})}$ . A limited sample  $I^{(\text{expr})}$  is taken from the same angle range, therefore:  $\{2\theta_{m+1}^{(\text{expr})} \dots 2\theta_{m+k}^{(\text{expr})}\} \equiv \{2\theta_1^{(\text{mod})} \dots 2\theta_k^{(\text{mod})}\}$ . We assign the value of the Gaussian function  $I^{(\text{mod})}$  to each discrete reflection intensity value from the model sample:

$$I_k^{(\text{mod})} = I_0 e^{-\frac{(2\theta_{m+k}^{(\text{mod})} - 2\theta_{m+k_0}^{(\text{mod})})^2}{2\sigma^2}} \quad (1)$$

where  $\sigma^2$  is the dispersion;  $k_0$  is the index at which the reflection angle  $2\theta$  corresponds to the maximum number of counts in a given range.

The sum of pairwise products of intensity values from the model  $I^{(\text{mod})}$  and from the experimental  $I^{(\text{expr})}$  samples at the corresponding angle values gives a number characterizing the degree of correlation between the model and experimental data. The resulting number  $S_0$  will be called the initial value of the degree of correlation. According to the definition, this value has the form of a sum:

$$S_0 = \sum_{l=1}^{l=k} I_l^{(\text{mod})} I_{m+l}^{(\text{expr})} \quad (2)$$

If two intensity values in the experimental sample are randomly permuted, we obtain

$$\begin{aligned} I_r^{(\text{prm})} &= \pi(I_r^{(\text{expr})}) \\ &= \{I_m^{(\text{expr})} \dots I_{p(i)}^{(\text{expr})} \dots I_{p(j)}^{(\text{expr})} \dots I_{m+k}^{(\text{expr})}\} \rightarrow \\ &= \{I_m^{(\text{expr})} \dots I_{p(j)}^{(\text{expr})} \dots I_{p(i)}^{(\text{expr})} \dots I_{m+k}^{(\text{expr})}\}, \quad (3) \end{aligned}$$

where  $\pi$  is the permutation function,  $p(i)$  and  $p(j)$  are the indices of randomly selected array elements.

The new sum of pairwise products of intensity values from the model and the experimental sample changed in accordance with formula (3) is  $S_{\text{prm } j} = \sum_{l=1}^{l=k} I_l^{(\text{mod})} I_{m+l}^{(\text{prm})}$ . The resulting number  $S_{\text{prm } j}$  will be called the current value of the degree of correlation.

The numerical value of the difference between the current degree of correlation and the initial value will be called the  $L_j$  parameter. In accordance with the definition, this parameter takes the form:  $L_j = |S_{\text{prm } j} - S_0|$ . A larger value of the

parameter  $L_j$  corresponds to a larger correlation value between two samples  $I^{(\text{expr})}$  and  $I^{(\text{mod})}$ . Let us carry out a large number (more than  $10^5$  values) of permutations using a pseudorandom number generator in the experimental sample. For each current value of the degree of correlation, we obtain the corresponding values of the  $L_j$  parameter. The obtained current values of the  $L_j$  parameter are accumulated on a histogram. If a maximum is formed on the histogram, then the value of the  $L_{\text{max}}$  parameter is assigned to the intensity value on the correlation pattern. If there is no maximum in the histogram, the value 0 is assigned to the intensity value. Thus, the intensity values on the correlation pattern are:

$$I_i^c = \begin{cases} L_{\text{max}}, & \text{if } \exists L_{\text{max}} \\ 0, & \text{if } 0 = \exists 0/L_{\text{max}} \end{cases} \quad (4)$$

This processing algorithm is sequentially applied to each experimentally obtained intensity value  $I_i$  at the corresponding angle values  $2\theta_i$ . Thus, a correlation pattern is formed based on the  $\{2\theta_i; I_i^c\}$  array.

Subsequently, the correlation pattern is used to identify phases using well-known software, for example, Match! current version is 3.16, developed by Crystal Impact (Germany) (Putz, 2023). The Crystallography Open Database (COD) diffraction database was used (Duée et al., 2019).

### D. Selection of weak $\alpha$ -quartz reflections and angle ranges for their recording

From all the reflections of  $\alpha$ -quartz, we chose five reflections with a low relative intensity. The values of interplanar distances ( $d$ ), angles ( $2\theta$ ), and normalized intensities of these reflections ( $I$ ) are given in Table I. These are both data obtained by us earlier (Skorbun et al., 2019) and data from the COD database (Machatschki, 1936; Kroll and Milko, 2003). The values of the intensities (normalized to 1000) of the selected reflections are in the range 4.1–28.1 rel. units. For subsequent experiments, the following intervals of  $2\theta$  angles were chosen: 55.2–56.2°, 63.8–65.0°, 73.2–74.2°, and 79.5–82.0°, taking into account the positions of the selected reflections on the diffraction pattern.

## III. RESULTS

### A. Characterization of the diffractometer background

First, we measured the background intensity of the diffractometer. To do this, we conducted measurements on the diffractometer without a sample in the selected angle intervals. Then, we processed the obtained data using our data processing method (Skorbun et al., 2019). Characteristics of the diffractometer background  $I_{b-\text{max}}$ ,  $I_{b-\text{min}}$ ,  $(I_{b-\text{max}} - I_{b-\text{min}})$ ,  $\langle I_b \rangle$ ,  $\sigma_b$ , and  $\Delta I_b$  on the diffraction pattern and  $I_b^c$ ,  $2\theta_b^c$  on the correlation pattern are shown in Table II. A segment of the diffraction pattern is shown in Figure 1(a). A segment of the correlation pattern is shown in Figure 1(b) (results of diffraction data processing by the data processing method).

The dependence of the background intensity on the angle has the form of a wide band [Figure 1(a)]. It has a constant component and a “noise” component. For each angle interval (Table II, column 2), the maximum background intensity values  $I_{b-\text{max}}$  (column 3) are in the range of 21.2–25.5 counts, the

TABLE I. Interplanar distance  $d$ , angles  $2\theta$ , and normalized intensities  $I$  of low-intensity  $\alpha$ -quartz reflections

No.	Authors experiment (Skorburn et al., 2019)			COD 96-101-1777 (Machatschki, 1936)			COD 96-153-2513 (Kroll and Milko, 2003)		
	$d$ , Å	$2\theta$ , °	$I$ , rel. units	$d$ , Å	$2\theta$ , °	$I$ , rel. units	$d$ , Å	$2\theta$ , °	$I$ , rel. units
1	2	3	4	5	6	7	8	9	10
1.	1.6530	55.60	5.2	1.6571	55.45	15.0	1.6537	55.58	16.7
2.	1.4482	64.30	7.4	1.4506	64.21	15.2	1.4477	64.65	17.6
3.	1.2855	73.70	7.4	1.2865	73.63	17.4	1.2838	73.81	22.2
4.	1.1975	80.15	10.5	1.1975	80.15	25.1	1.1952	80.34	28.1
5.	1.1950	80.35	4.1	1.1946	80.38	8.1	1.1926	80.55	8.3

TABLE II. Characteristics of the diffractometer background  $I_{b-max}$ ,  $I_{b-min}$ ,  $I_{b-max} - I_{b-min}$ ,  $\langle I_b \rangle$ ,  $\sigma_b$ ,  $\Delta I_b$ , and background pseudo-reflections  $I_b^c$ ,  $2\theta_b^c$  obtained by data processing method (counting time 195 s, diffractometer without a specimen)

No.	Angle interval, °	$I_{b-max}$ , counts	$I_{b-min}$ , counts	$I_{b-max} - I_{b-min}$ , counts	$\langle I_b \rangle$ , counts	$\sigma_b$ , counts	$\Delta I_b$ , counts	$I_b^c$ , counts	$2\theta_b^c$ , °
1	2	3	4	5	6	7	8	9	10
1.	55.2–56.2	21.2	8.9	12.3	14.6	3.7	14.8	1.6	55.6
2.	63.8–65.0	22.7	8.0	14.7	14.9	3.5	14.0	3.5	64.7
3.	73.2–74.2	25.5	8.9	16.6	16.6	4.0	16.0	3.6	73.5
4.	79.5–82.0	25.2	5.6	19.6	14.2	4.6	18.4	4.0	81.3

minimum  $I_{b-min}$  (constant component) – 5.6–8.9 counts, their difference  $I_{b-max} - I_{b-min}$  (noise component, column 5) 12.3–19.6 counts. With this approach, the background components depend on specific maximum and minimum values. We will try to use all background values within the same angle interval. Let us find the average values of the background intensities  $\langle I_b \rangle$  (Table II, column 6) and standard deviations

$\sigma_b$  (column 7). The amplitude of the “noise” component of the background  $\Delta I_b$  (column 8) is equal to the quadruple standard deviation of the background average intensity values in accordance with the formula  $\Delta I_b = 4\sigma_b$ . In the range of values from  $\langle I_b \rangle - 2\sigma_b$  to  $\langle I_b \rangle + 2\sigma_b$ , the background intensities are found with a probability of 95.4%. This is clearly seen in Figure 1(a). Of the 40 experimental points shown in the figure, 38 points are located inside the band with a “width” of  $4\sigma_b$ , i.e. 95%. Now the characteristics of the background are practically independent of specific maximum and minimum values. They are determined considering the entire data array for a given angle interval.

A segment of the correlation pattern was obtained by applying our data processing method to the diffraction pattern [Figure 1(b)]. The constant component of the background was “cut off”, and the “noise” component was converted into several pseudo-reflections. The intensity values of pseudo-reflections  $I_b^c$  (Table II, column 9) for all angle intervals do not exceed four counts.

We see (Table II) that the average values of the background intensity of the diffractometer  $\langle I_b \rangle$  (column 6) and the values of the “noise” component of the background  $\Delta I_b$  (column 8) are in the range of 14.2–16.6 counts and 14.0–18.4 counts, respectively, for all angle intervals with the counting time of 195 s. In this case, applying the method of processing diffraction data to the intensities of the diffractometer background for a range of angles gives pseudo-reflections  $I_b^c$  (column 9) with an intensity of up to four counts.

### B. Determination of signal-to-noise ratios for weak $\alpha$ -quartz reflections

Next, we mounted a specimen of  $\alpha$ -quartz on a diffractometer. Measurements were carried out in the intervals of angles No. 1–4 (see Table III, column 2). Table III presents the obtained characteristics of  $\alpha$ -quartz and background reflections: (intensities and angles):  $I_q^d$ ,  $2\theta_q^d$ ,  $\langle I_b \rangle$ ,  $\sigma_b$ ,  $\Delta I_b$ , and  $I_q^d/\Delta I_b$  signal-to-noise ratios. The resulting data were then processed using our data processing method. The obtained

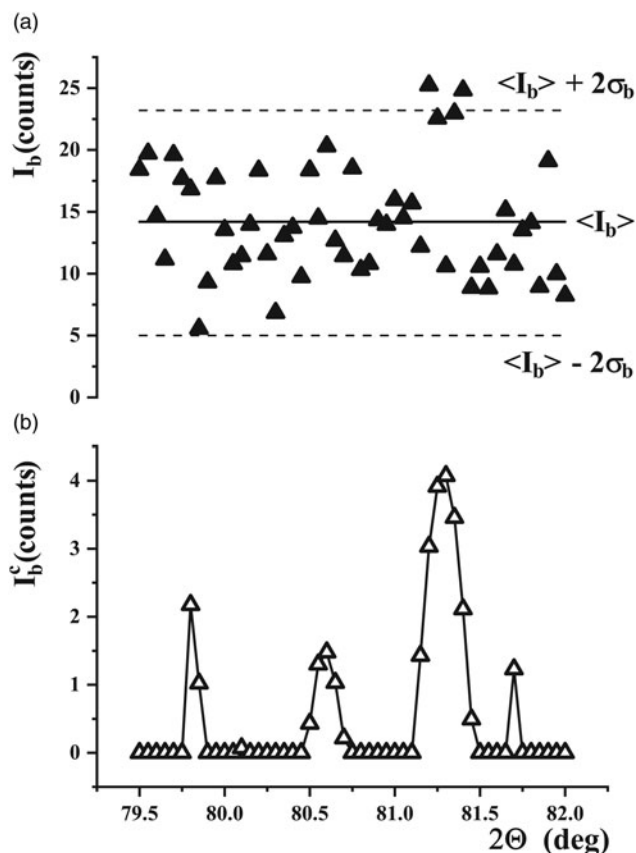


Figure 1. Segments of diffraction [Figure 1(a)] and correlation [(Figure 1(b))] patterns of the diffractometer background (counting time 195 s).

TABLE III. Characteristics of  $\alpha$ -quartz reflections  $I_q^d$ ,  $2\theta_q^d$ , and background  $\langle I_b \rangle$ ,  $\sigma_b$ ,  $\Delta I_b$ , as well as  $\alpha$ -quartz reflections  $I_q^c$ ,  $2\theta_q^c$ , and background pseudo-reflections  $I_b^c$  obtained by the method data processing;  $I_q^d/\Delta I_b$  ratios (counting time 195 s,  $\alpha$ -quartz specimen on the diffractometer)

No	Angle interval, °	$I_q^d$ , Counts	$2\theta_q^d$ , °	$I_q^c$ , counts	$2\theta_q^c$ , °	$\langle I_b \rangle$ , counts	$\sigma_b$ , counts	$\Delta I_b$ , counts	$I_b^c$ , counts	$I_q^d/\Delta I_b$
1	2	3	4	5	6	7	8	9	10	11
1.	55.2–56.2	20.0 ± 3.5	55.46 ± 0.02	10.5	55.45 ± 0.02	19.7	2.7	10.8	1.5	1.85
2.	63.8–65.0	14.9 ± 2.4	64.15 ± 0.03	7.5	64.15 ± 0.02	17.6	2.4	9.6	1.5	1.55
3.	73.2–74.2	24.7 ± 4.2	73.62 ± 0.02	11.0	73.65 ± 0.02	17.8	3.8	15.2	3.7	1.63
4.	79.5–82.0	27.2 ± 3.5	80.10 ± 0.02	11.7	80.10 ± 0.02	20.8	3.5	14.0	0.0	1.94
		35.9 ± 8.8	81.54 ± 0.02	9.4	81.60 ± 0.02	27.5	2.2	8.8	0.0	4.10

Note: the half-width of reflections ( $\beta$ ) was 0.3°.

characteristics of  $\alpha$ -quartz reflections  $I_q^c$ ,  $2\theta_q^c$  and background pseudo-reflections  $I_b^c$  are also shown in Table III. A segment of the diffraction pattern with the reflection of  $\alpha$ -quartz is presented in Figure 2(a), correlation pattern – in Figure 2(b). Nonlinear curve fit of each reflection of  $\alpha$ -quartz to a Gaussian function was carried out on the diffraction pattern [Figure 2(a)].

The values of the intensities of the  $\alpha$ -quartz reflections  $I_q^d$ , determined by the nonlinear curve fit to a Gaussian function, are in the range of 14.9–35.9 counts (Table III, column 3). The values of the  $2\theta_q^d$  angles are presented in column 4. The values of the intensities of  $\alpha$ -quartz reflections after applying our method of data processing on the correlation pattern  $I_q^c$  (column 5) are 7.5–11.7 counts, which is  $\sim 2$  times less than the intensity of  $\alpha$ -quartz reflections  $I_q^d$  (column 3). The angles  $2\theta_q^c$  at which the reflections are located on the correlation pattern (column 6), correspond to the values on the diffraction

pattern (column 4) taking into account the determination error. The average background intensities  $\langle I_b \rangle$  increased 1.5 times to 17.3–27.5 counts (column 7) compared with the average values of the background intensities of the diffractometer (Table II, column 6). This is due to the fact that scattering from the  $\alpha$ -quartz specimen also contributes to the background intensity. Standard deviations of the background intensity values  $\sigma_b$  (column 8) decreased to 2.2–3.8 counts, and the values of the background “noise” component  $\Delta I_b$  (column 9) decreased to 8.8–15.2 counts. The intensity values of pseudo-reflections after applying the data processing method ( $I_b^c$ ) (column 10) do not exceed four counts. After applying the data processing method, the reflection intensities of  $\alpha$ -quartz  $I_q^c$  (column 5) significantly exceed the intensities of pseudo-reflection  $I_b^c$  (column 10), which indicates their high reliability. The ratios of the reflection intensities of  $\alpha$ -quartz  $I_q^d$  (column 3) to the values of the “noise” component of the background  $\Delta I_b$  (column 9) are in the range of 1.55–4.10 (column 11), i.e. the intensity of reflections of  $\alpha$ -quartz is significantly greater than the value of the “noise” component of the background  $\Delta I_b$ . Visually, this is manifested in the fact that the reflections of  $\alpha$ -quartz stand out above the background [Figure 2(a)].

The signal-to-noise ratios for weak  $\alpha$ -quartz reflections are significantly greater than 1. In this case, the  $\alpha$ -quartz reflections stand out above the background. The data processing method reliably identifies  $\alpha$ -quartz reflections. The intensity of  $\alpha$ -quartz reflections is significantly greater than the intensity of background pseudo-reflections.

### C. Increasing background characteristics due to an additional source of $\gamma$ -quanta from brown LFCM ceramics

A specimen of LFCM brown ceramics was placed near the cuvette with a specimen of  $\alpha$ -quartz. This was done to increase the background due to  $\gamma$ -quanta, which are emitted by LFCM radionuclides. Then, the intervals of angles were chosen, in which there are no reflections of  $\alpha$ -quartz. This made it possible to measure the background in the presence of the LFCM specimen. The selected angle intervals are shown in Table IV (column 2). It can be seen that for a counting time of 195 s, all indicators such as: average values of the background intensity  $\langle I_b \rangle$  (column 4), standard deviations of the values of the background intensity  $\sigma_b$  (column 5), values of the “noise” component of the background ( $\Delta I_b$ , column 6) – increased compared to the values of the corresponding parameters of the background of the diffractometer without specimens of  $\alpha$ -quartz and brown ceramics (see Table II). The average value of the background  $\langle I_b \rangle$  (column 4)

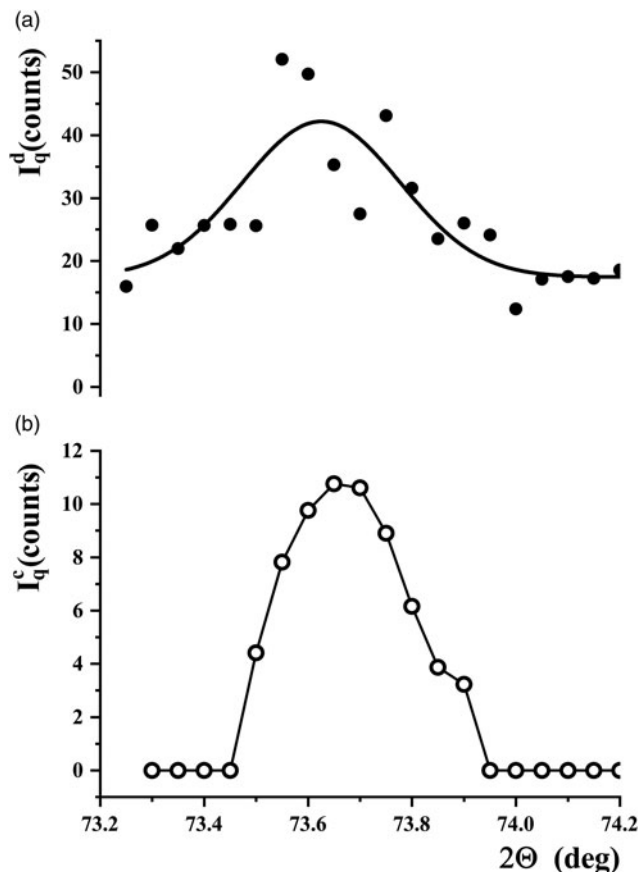


Figure 2. Segments of the diffraction pattern [(Figure 2(a)) and correlation pattern [(Figure 2(b)) of  $\alpha$ -quartz reflection (counting time 195 s).

TABLE IV. Characteristics of the diffractometer background  $\langle I_b \rangle$ ,  $\sigma_b$ ,  $\Delta I_b$ , and background pseudo-reflections  $I_b^c$ ,  $2\theta_b^c$  obtained by data processing (counting time ( $t$ ) 65 and 195 s; specimens of  $\alpha$ -quartz and LFCM brown ceramics are on the diffractometer).

No	Angle interval, °	$t$ , s	$\langle I_b \rangle$ , counts	$\sigma_b$ , counts	$\Delta I_b$ , counts	$I_b^c$ , counts	$2\theta_b^c$ , °
1	2	3	4	5	6	7	8
1.	7.0–10.0	65	13.3	2.9	11.6	1.2	9.35
		195	39.9	4.8	19.2	4.5	8.20
2.	61.0–63.0	65	9.2	1.9	7.6	2.0	61.95
		195	28.2	3.7	14.7	2.7	61.90
3.	69.0–71.0	65	9.4	2.6	10.4	1.4	69.75
		195	28.7	4.6	18.4	2.5	69.30
4.	78.0–80.0	65	11.1	3.9	15.6	0.6	79.25
		195	29.4	6.1	24.4	2.1	78.85

increased significantly by 1.7–1.9 times, and the values of the “noise” component of the background  $\Delta I_b$  (column 6) did not increase significantly – by 1.05–1.17 times. After applying our data processing method, the value of the intensity of pseudo-reflections  $I_b^c$  (column 7) also does not exceed values of more than four counts for a counting time of 195 s (except one value in the range of angles 7.0–10.0). The positions of pseudo-reflections after applying the data processing method (the corresponding angles ( $2\theta_b^c$ )) for one interval of angles do not match as they should be (see Table IV, column 8). The correlation pattern with background pseudo-reflections is shown in Figure 3(b).

Thus, the average value of the background intensity and the value of the “noise” component of the background increased due to the use of an additional source of  $\gamma$ -quanta from brown LFCM ceramics.

#### D. Determination of signal-to-noise ratios for weak $\alpha$ -quartz reflections with enhanced background

Now we have returned to the same angle intervals (see Table III, column 2), which contain reflections of  $\alpha$ -quartz. The measurements were carried out at three counting times (Table V, column 3). We have obtained reflections of  $\alpha$ -quartz. One of the diffraction patterns is shown in Figure 4(a), and a correlation pattern in Figure 4(b). We see that, as it should be, for each angle interval with an increase in the recording time from 65 to 195 s and up to 390 s, the reflection intensity increases by  $\sim 3$  and  $\sim 6$  times (column 4). The values of the angles  $2\theta_q^d$  corresponding to them practically coincide, taking into account the data processing error (column 5). After applying the data processing method  $I_q^c$  (column 6), the reflection intensities are  $\sim 2$  times less than the reflection intensities of  $\alpha$ -quartz  $I_q^d$  for each of the three counting times in all angle intervals (column 4). The values of the angles corresponding to them  $2\theta_q^c$  (column 7) practically coincide with the angles for reflections of  $\alpha$ -quartz  $2\theta_q^d$  (column 5). The average values of the background intensities  $\langle I_b \rangle$  (column 8) increase by  $\sim 3$  and  $\sim 6$  times for each angle interval with increasing recording time from 65 to 195 s and up to 390 s. The values of the “noise” component of the background  $\Delta I_b$  (column 10) also increase, but to a lesser extent. The maximum intensity of pseudo-reflections after applying the data processing method  $I_b^c$  (column 11) does not exceed 2.4 counts. After using the data processing method, the maximum

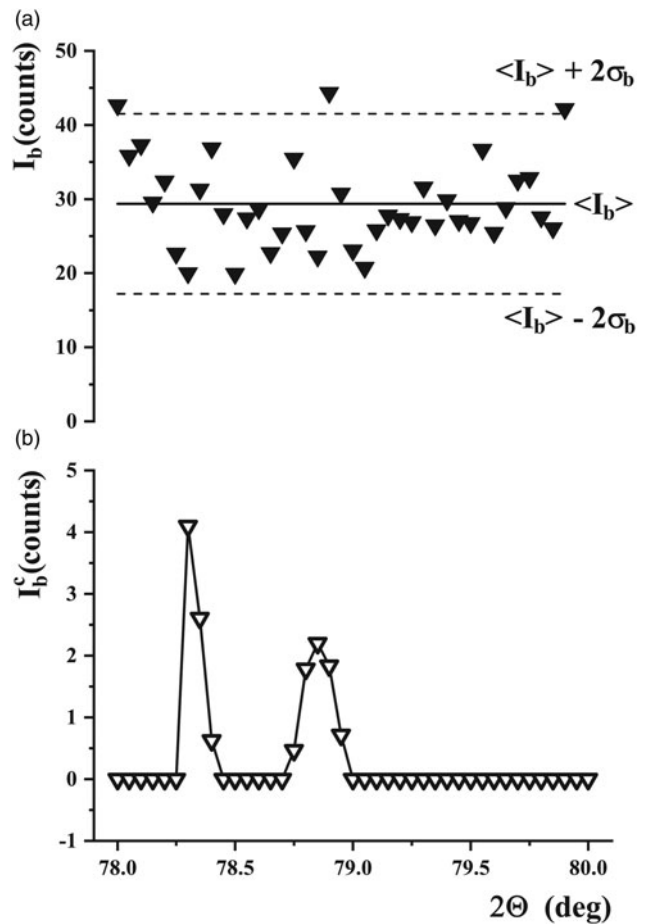


Figure 3. Segments of the diffraction pattern [(Figure 3(a))] and correlation pattern [(Figure 3(b))] of the background from the diffractometer with specimens of  $\alpha$ -quartz and brown ceramics LFCM (counting 195 s).

intensity of background reflections  $I_b^c$  (column 11) does not exceed 2.4 counts for a counting time of 65 s; 5.7 counts (greater than 4, outlier) for a counting time of 195 s and 8.0 counts for a counting time of 390 s, respectively. The ratio of the reflection intensity of  $\alpha$ -quartz to the values of the “noise” component of the background  $I_q^d/\Delta I_b$  (column 13) ranges from 0.56 to 1.94. By changing the counting time, we can change the ratio of the reflection intensity values of  $\alpha$ -quartz to the values of the “noise” component of the background  $I_q^d/\Delta I_b$ .

Average background intensities  $\langle I_b \rangle$  for the  $\alpha$ -quartz and the brown LFCM ceramic specimens (Table V, column 8, counting time 195 s) compared to the average background intensities for the  $\alpha$ -quartz specimen without the brown LFCM ceramic specimen (Table III, column 7) increased by an average of  $\sim 1.4$  times due to the use of the brown LFCM ceramic specimen as a source of “noise” gamma quanta.

The values of the “noise” component of the background  $\Delta I_b$  for a specimen of  $\alpha$ -quartz with a specimen of brown ceramics LFCM (Table V, column 10, counting time 195 s) compared with the values of the “noise” component of the background for the specimen of  $\alpha$ -quartz without the specimen of brown ceramics LFCM (Table III, column 9) increased by an average of  $\sim 1.7$  times due to the use of the specimen of brown ceramics.

We see [Figure 4(a)] that the reflection of  $\alpha$ -quartz in the range of angles 63.8–64.8° at a counting time of 195 s, stands out well against the noise component of the background (the

TABLE V. Characteristics of  $\alpha$ -quartz reflections  $I_q^d$ ,  $2\theta_q^d$ , and background ( $I_b$ ),  $\sigma_b$ ,  $\Delta I_b$ ;  $\alpha$ -quartz reflections  $I_q^c$ ,  $2\theta_q^c$ , and background pseudo-reflections  $I_b^c$  obtained by data processing; ratios  $I_q^d/\Delta I_b$  (counting time ( $t$ ) 65, 195 and 390 s, specimens of  $\alpha$ -quartz and brown LFCM ceramics on the diffractometer)

No	Angle interval, °	$t$ , s	$I_q^d$ , counts	$2\theta_q^d$ , °	$I_q^c$ , counts	$2\theta_q^c$ , °	$\langle I_b \rangle$ , counts	$\sigma_b$ , counts	$\Delta I_b$ , counts	$I_b^c$ , counts	$2\theta_b^c$ , °	$I_q^d/\Delta I_b$	
1	2	3	4	5	6	7	8	9	10	11	12	13	
1.	55.2–56.2	65	5.9 ± 1.8	55.41 ± 0.02	2.7	55.40	10.5	2.5	10.0	1.0	55.80	0.59	
		195	17.9 ± 4.6	55.40 ± 0.02	8.5	55.40	28.4	4.7	18.8	2.5	55.80	0.95	
		390	38.1 ± 6.4	55.42 ± 0.01	18.0	55.40	57.6	6.3	25.2	7.5	55.80	1.51	
2.	63.8–65.0	65	6.4 ± 1.4	64.24 ± 0.03	3.3	64.15	10.5	2.2	8.8	2.4	64.50	0.73	
		195	16.9 ± 3.7	64.17 ± 0.04	7.7	64.15	25.4	4.3	17.2	3.5	64.55	0.98	
		390	32.8 ± 5.5	64.19 ± 0.03	17.5	64.15	52.6	5.3	21.2	8.0	64.50	1.55	
3.	73.2–74.2	65	6.1 ± 2.0	73.70 ± 0.05	2.0	73.65	11.5	2.7	10.8	2.2	73.90	0.56	
		195	17.9 ± 3.5	73.64 ± 0.03	8.0	76.60	28.6	3.8	15.2	5.7 <sup>a</sup>	73.90	1.18	
		390	55.3 ± 9.3	80.09 ± 0.03	23.0	80.15	58.6	8.2	32.8	–	–	1.69	
4.	79.5–82.0	65	– <sup>b</sup>	–	3.0	81.60	9.6	2.8	11.2	–	–	–	
		195	32.2 ± 9.3	81.55 ± 0.02	12.5	81.60	29.6	5.1	20.4	–	–	1.58	
		390	63.7 ± 16.8	81.55 ± 0.01	25.0	81.60	58.6	8.2	32.8	–	–	1.94	
		–	–	–	–	–	–	–	–	–	–	–	–
		–	–	–	–	–	–	–	–	–	–	–	–

Note: half-width of reflections ( $\beta$ ) is equal to 0.3°.

<sup>a</sup>Spike.

<sup>b</sup>Experimental data did not fit to a Gaussian function.

ratio of the intensity of  $\alpha$ -quartz reflection to the values of the “noise” component of the background  $I_q^d/\Delta I_b$  is 0.98). After applying our method of processing diffraction data [Figure 4 (b)], this reflection is recorded with high reliability in the correlation pattern (its intensity is greater than 4 counts).

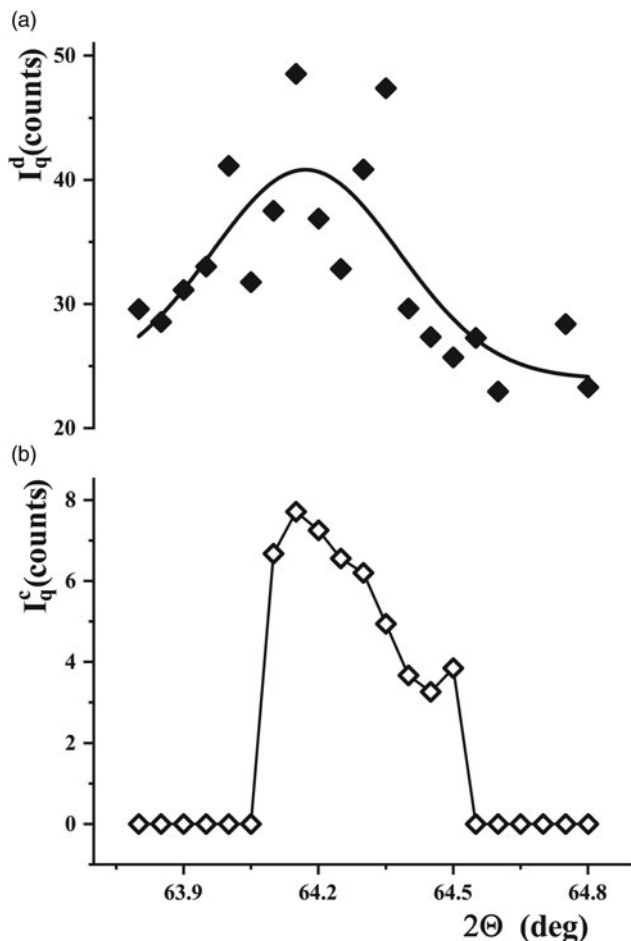


Figure 4. Segments of the diffraction pattern [(Figure 4(a)) and correlation pattern [(Figure 4(b)) of  $\alpha$ -quartz with brown ceramics (counting time 195 s).

The signal-to-noise ratios for weak  $\alpha$ -quartz reflections were reduced to 0.95–1.58 at a counting time of 195 s compared to the previously obtained values of 1.55–4.1 in section 5.3. This was possible due to an increase in the intensity of the “noise” component of the background using an additional source of  $\gamma$ -quanta from brown LFCM ceramics.

The best results in this section are signal-to-noise ratios of 0.56–0.73 (significantly less than 1). These were obtained with a counting time of 65 s (see Table V, angle intervals No. 1, 2 and 3).

### E. Identifying the $\alpha$ -quartz reflection with a signal-to-noise ratio less than 1. Refinement of characteristics

Next, let us pay attention to the cases when the intensity of reflections of  $\alpha$ -quartz  $I_q^d$  (Table V, column 4) is less than the “noise” component of the background  $\Delta I_b$  (Table V, column 10). These are the angle intervals 55.2–56.2, 63.8–65.0, and 73.2–74.2°, counting time 65 s. In this case, the ratio of the intensity of  $\alpha$ -quartz reflection to the values of the “noise” component of the background  $I_q^d/\Delta I_b$  is in the range of 0.56–0.73. Let’s choose one of the cases – the interval of angles 63.8–65.0° with a counting time of 65 s.

We took six measurements in this range of angles with a counting time of 60 s. The  $I_q^d$ ,  $2\theta_q^d$  characteristics of  $\alpha$ -quartz reflections, also  $I_q^c$ ,  $2\theta_q^c$  after applying the data processing method, are presented in Table VI (angle interval 63.8–64.8°, counting time 60 s).

We see (Table VI, column 2) that the intensity of  $\alpha$ -quartz reflections  $I_q^d$  is 5.88–8.07 counts. The average  $\langle I_q^d \rangle$  value is  $6.77 \pm 0.8$  counts. The angles corresponding to these reflections are in the range of 64.15–64.27°. The average value is  $64.17 \pm 0.04$ °. After applying our method of processing X-ray diffraction data, the reflection intensities  $I_q^c$  are in the range of 2.73–5.04 counts. The average  $\langle I_q^c \rangle$  value is  $3.03 \pm 1.08$  counts. The angles  $2\theta_q^c$  corresponding to these reflections are in the same range of 64.14–64.27°. The average value is  $64.22 \pm 0.05$ °. After applying the method, the reflection intensity

TABLE VI. Characteristics of  $\alpha$ -quartz reflections  $I_q^d$ ,  $2\theta_q^d$ , and  $I_q^c$ ,  $2\theta_q^c$  obtained by data processing (in the angle interval  $63.8\text{--}64.8^\circ$  with a counting time of 60 s, the specimens of  $\alpha$ -quartz and brown LFCM ceramics are on a diffractometer)

No	$I_q^d$ , counts	$2\theta_q^d$ , °	$I_q^c$ , counts	$2\theta_q^c$ , °
1	2	3	4	5
1.	6.52	64.18	1.75	64.24
2.	7.29	64.15	3.04	64.25
3.	6.35	64.24	2.73	64.24
4.	6.51	64.15	2.79	64.27
5.	5.88	64.17	2.82	64.21
6.	8.07	64.15	5.04	64.14
$\langle \rangle$	6.77	64.17	3.03	64.22
$\sigma$	0.80	0.04	1.08	0.05

Note:  $\langle \rangle$  denotes average values of  $I_q^d$ ,  $2\theta_q^d$ ,  $I_q^c$ ,  $2\theta_q^c$ .

decreased by 2.2 times, and the average values of the reflection angles did not change (considering the measurement error).

For subsequent use, we chose the  $\alpha$ -quartz reflection in the angle range of  $63.8\text{--}64.8^\circ$  with a counting time of 60 s. The refined reflection intensity is  $6.77 \pm 0.8$  counts.

### F. Determination of the signal-to-noise ratio values at which the data processing method allows the $\alpha$ -quartz reflection to be separated from the background noise component

To elucidate the possibilities of our method of processing X-ray diffraction data, we recorded the reflections of  $\alpha$ -quartz in the angle range of  $63.8\text{--}64.8^\circ$  at different counting times (reducing the counting time from 60 to 5 s), thereby providing the ratio of the intensity of  $\alpha$ -quartz reflection to the values of the “noise” component of the background  $I_q^d/\Delta I_b$  less than 0.73 (Table V, column 13). The characteristics of the background were determined from the recording results in the angle range  $61.0\text{--}63.0^\circ$ . Reflection intensities of  $\alpha$ -quartz  $I_q^d$ , reflection intensities after applying the data processing method  $I_q^c$ , mean background intensities  $\langle I_b \rangle$ , background standard deviation average background intensity  $\sigma_b$ , values of the “noise” component of the background  $\Delta I_b$ , the maximum intensity of pseudo-reflections after applying the data

processing method  $I_{b-\max}$  and the ratio of the reflection intensity of  $\alpha$ -quartz to the values of the background “noise” component  $I_q^d/\Delta I_b$  are presented in Table VII. The counting time during recording (Table VII, column 2) was gradually reduced from 60 to 5 s. The intensity of  $\alpha$ -quartz reflections  $I_q^d$  for a counting of 60 s is taken from Table VI, column 2, row “average”. For all smaller countings, the reflections’ intensity is calculated proportionately to the shorter counting time. Naturally, the intensity of reflections (column 3) decreases with decreasing counting time. The intensity of  $\alpha$ -quartz reflections after applying our data processing method  $I_q^c$  (column 4) is practically independent of the counting time. The average values of the background intensities  $\langle I_b \rangle$  (column 5), the standard deviation of the background  $\sigma_b$  (column 6), and the values of the “noise” component of the background  $\Delta I_b$  (column 7) show a slight tendency to increase with decreasing counting time. After applying the data processing method  $I_q^c$  (column 8), the maximum intensity value of pseudo-reflections shows a larger increase with decreasing counting time. The ratio of the intensity of  $\alpha$ -quartz reflection to the values of the “noise” component of the background  $I_q^d/\Delta I_b$  (column 9) decreases almost monotonically with decreasing counting time.

Analysis of the data in Table VII shows that for each counting time in the interval from 60 to 45 s, the intensities of  $\alpha$ -quartz reflection  $I_q^d$  (column 3) are larger than the reflection intensities after applying the data processing method  $I_q^c$  (column 4), and these reflection intensities ( $I_q^c$ , column 4) are in turn greater than the maximum values of the intensity of pseudo-reflections after applying the data processing method  $I_b^c$  (column 8). In this counting time interval, the intensities of  $\alpha$ -quartz reflections on the diffraction and correlation patterns exceed the intensities of pseudo-reflections after applying our data processing method. This indicates that the method of processing X-ray diffraction data reliably reveals reflections of  $\alpha$ -quartz from the “noise” component of the background.

For each counting time in the interval from 40 to 25 s, the intensity of reflections of  $\alpha$ -quartz  $I_q^d$  (column 3), the reflection intensity after applying the data processing method  $I_q^c$  (column 4), and the maximum values of the intensity of pseudo-reflections after applying the processing method  $I_b^c$  (column 8) have similar values. This indicates that at this counting time interval it

TABLE VII. Characteristics of reflections of  $\alpha$ -quartz  $I_q^d$  and background  $\langle I_b \rangle$ ,  $\sigma_b$ ,  $\Delta I_b$ ; reflections of  $\alpha$ -quartz  $I_q^c$  and pseudo-reflections of background  $I_b^c$ , obtained by data processing; the relationship  $I_q^d/\Delta I_b$  (counting time 60 – 5 s, angle interval  $63.8\text{--}64.8^\circ$ , background in the angle interval  $61.0\text{--}63.0^\circ$ , specimens of  $\alpha$ -quartz and LFCM brown ceramics are on a diffractometer)

No	$t, s$	$I_q^d$ , counts	$I_q^c$ , counts	$\langle I_b \rangle$ , counts	$\sigma_b$ , counts	$\Delta I_b$ , counts	$I_b^c$ , counts	$I_q^d/\Delta I_b$
1	2	3	4	5	6	7	8	9
1.	60	6.8	4.0	13.1	2.4	9.6	2.8	0.71
2.	55	6.2	4.2	13.4	2.6	10.4	3.3	0.60
3.	50	5.6	2.8	12.8	3.1	12.4	1.9	0.45
4.	45	5.1	4.8	14.0	3.4	13.6	1.6	0.38
5.	40	4.5	3.1	13.8	3.8	15.2	4.7	0.30
6.	35	4.0	4.4	13.1	3.2	12.8	2.7	0.31
7.	30	3.4	3.1	13.5	4.1	16.4	3.7	0.21
8.	25	2.8	3.4	12.6	3.7	14.8	1.4	0.19
9.	20	2.3	4.6	13.4	5.6	22.4	4.6	0.10
10.	15	1.7	4.8	12.5	4.8	19.2	5.5	0.09
11.	10	1.1	5.5	13.7	6.6	26.4	5.8	0.04
12.	5	0.6	4.7	15.6	10.0	40.0	7.1	0.02

Note: The half-width of reflections ( $\beta$ ) is equal to  $0.3^\circ$ .

is difficult to assess the efficiency of the X-ray diffraction data processing method for separating the  $\alpha$ -quartz reflection from the “noise” component of the background.

For each counting time in the interval from 20 to 5 s, the intensities of  $\alpha$ -quartz reflection  $I_q^d$  (column 3) have lower values than the reflection intensities after applying our data processing method  $I_q^c$  (column 4) and the maximum values of the intensity of pseudo-reflections after applying the data processing method  $I_b^c$  (column 8). The intensity of reflections of  $\alpha$ -quartz on the diffraction pattern is less than the intensity of pseudo-reflections after applying the data processing method. This indicates that, in this counting interval, the method of processing X-ray diffraction data reveals  $\alpha$ -quartz reflections from the “noise” component of the background with low reliability.

Thus, the data in Table VII allow us to conclude that at the ratio of the intensity of  $\alpha$ -quartz reflection to the values of the “noise” component of the background  $I_q^d/\Delta I_b$  up to 0.38 (column 9, counting time 45 s), our method for processing of X-ray diffraction data makes it possible to reliably detect  $\alpha$ -quartz reflections from the “noise” component of the background. But when the ratio of the intensity of  $\alpha$ -quartz reflections to the values of the “noise” component of the background  $I_q^d/\Delta I_b$  is less than 0.10 (column 9, counting time 20 s), the above method does not allow this. For cases where the ratio of the intensity of reflections of  $\alpha$ -quartz to the values of the “noise” component of the background  $I_q^d/\Delta I_b$  is in the range of 0.30–0.19 (column 9, counting time 40–25 s), a deeper analysis of the data is required.

We plotted the intensity of  $\alpha$ -quartz reflections  $I_q^d$ , the intensity of reflections after applying the data processing method  $I_q^c$  and the maximum intensity of pseudo-reflections after applying the data processing method ( $I_{b-\max}$ ) versus counting time (Figure 5). Considering that after applying the data processing method, the reflection intensities  $I_q^d$  and the

maximum values of the intensity of pseudo-reflections  $I_q^c$  have a significant spread in values due to significant errors in their measurement, we constructed best-fit lines using the least square method for these intensities at time intervals of 60–25 s and 20–5 s.

Figure 5 shows that for a counting time interval of 60–25 s, the reflection intensities along the fit line after applying the data processing method ( $I_q^c$ , straight line 2) are greater than the maximum pseudo-reflection intensities after applying the data processing method ( $I_{b-\max}$ , straight line 3). While for a counting time interval of 20–5 s, the values along these linear splines change places (straight lines 4 and 5). This unambiguously indicates that in the range of counting times of 60–25 s, the method of processing X-ray diffraction data makes it possible to detect  $\alpha$ -quartz reflections from the “noise” component of the background with high reliability, and in the range of counting times of 20–5 s, it does not allow it.

Also, from the data in Figure 5, it follows that for a counting time interval of 40–25 s, the values along the fit line of the  $\alpha$ -quartz reflection intensity  $I_q^d$  (straight line 1) are comparable with the reflection intensity after applying the data processing method  $I_q^c$  (straight line 2). This indicates a low reliability of the existence of reflections determined by the method of processing X-ray diffraction data in this interval of recording times, i.e. for the ratio of the intensity of  $\alpha$ -quartz reflection to the values of the “noise” component of the background  $I_q^d/\Delta I_b$  equal to 0.3–0.19 (see Table VII).

Figure 6 shows segments of diffraction Figures 6(a), 6(c), and 6(f) and correlation Figures 6(b), 6(d), and 6(e) patterns of  $\alpha$ -quartz with brown ceramics. In Figure 6(a), with some difficulty, one can see the reflection of  $\alpha$ -quartz when its intensity is 0.6 of the noise component of the background. In Figures 6(c) and 6(e), it is no longer possible to see the reflection of  $\alpha$ -quartz (the intensity of the reflection of  $\alpha$ -quartz is 0.38 and 0.31 of the values of the noise component of the background). Moreover, the X-ray diffraction data processing method makes it possible to identify these reflections with confidence [Figures 6(b), 6(d), and 6(f)].

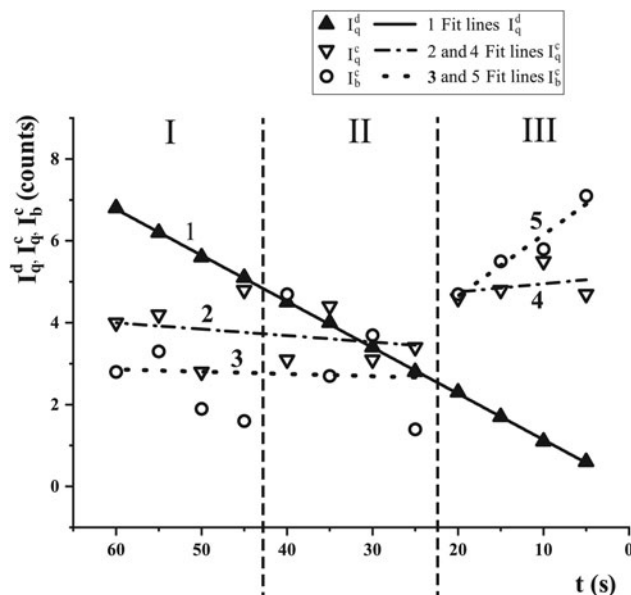


Figure 5. The intensity of reflections of  $\alpha$ -quartz on the diffraction pattern  $I_q^d$ , the intensity of the reflection on the correlation pattern after applying the data processing method  $I_b^c$ , and the maximum values of the intensity of pseudo-reflections after applying the data processing method  $I_q^c$  versus time counting. Fit lines:  $I_q^d$  – 1,  $I_q^c$  – 2 and 4 in the segments 60–25 s and 20–5 s,  $I_b^c$  – 3 and 5 in the segments 60–25 and 20–5 s, respectively.

#### IV. DISCUSSION AND ANALYSIS

The practice of using X-ray phase analysis method shows that the vast majority of researchers usually obtain data at a high signal-to-noise ratio (Guinebretière, 2007). If there is a need to work at a low signal-to-noise ratio, then much more often, one has to deal with reflections of low intensity due to a low content of crystalline phases with a significant number of these phases (up to eight or more). This situation occurs when we have studied the LFCM of the fourth block of the Chernobyl NPP (Gabelkov et al., 2023). Much less often, one has to deal with the need to work with reflections of low intensity due to the time limitation for obtaining data on the phase composition of the material, study of steel during its heat treatment) (Wiessner et al., 2021).

The signal-to-noise ratio can be increased by decreasing the noise values. This can be achieved by using a particularly sensitive low-noise detector (Taguchi et al., 2008). This method is more expensive than the method of processing X-ray diffraction data for multiphase materials with low-phase content.

In the case of studying multiphase materials with a low content for some of the phases, the signal-to-noise ratio can

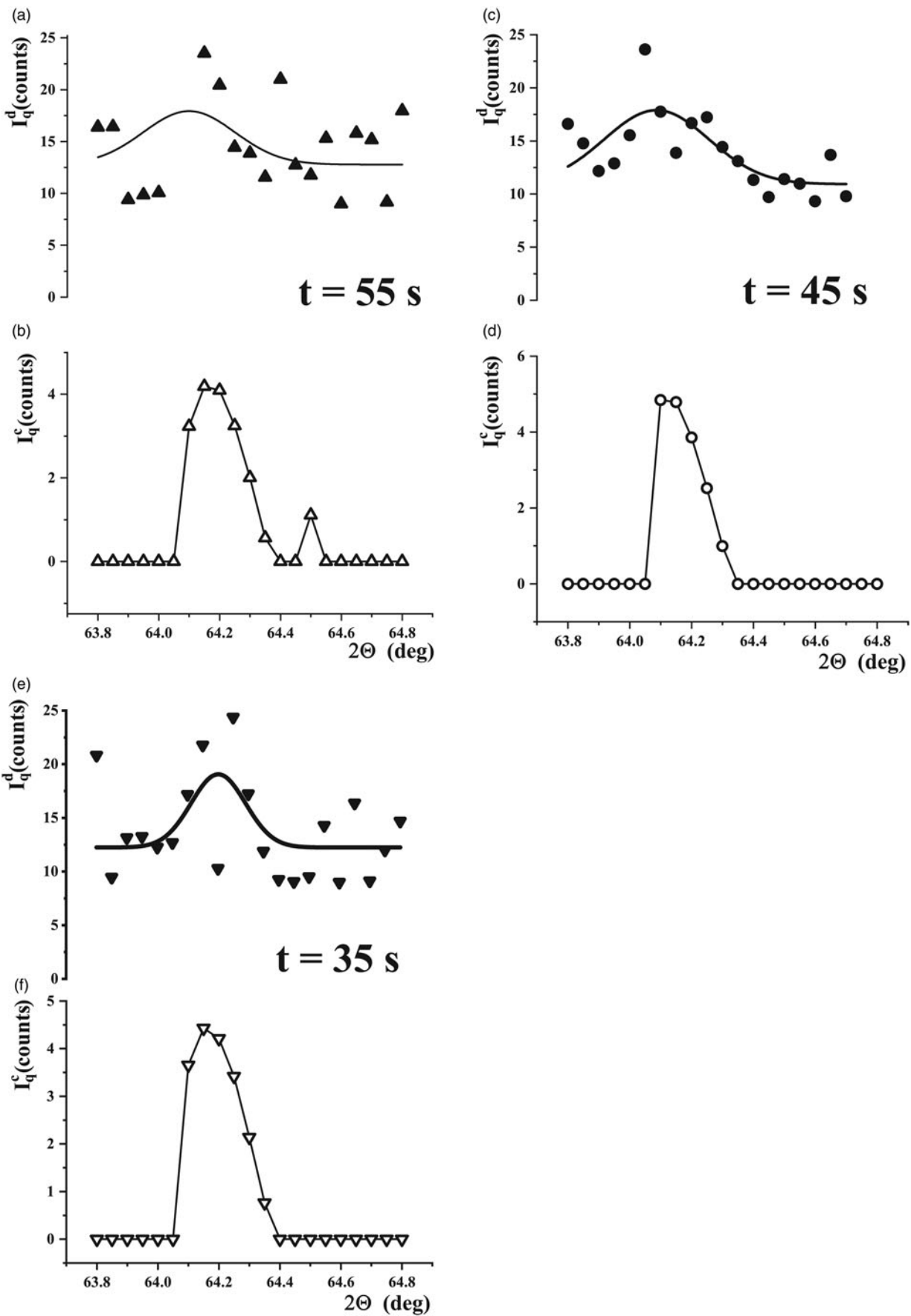


Figure 6. Segments of diffraction [Figures 6(a), 6(c), and 6(e)] and correlation [Figures 6(b), 6(d), and 6(f)] patterns of  $\alpha$ -quartz with brown ceramics (counting time: 55 s [Figures 6(a) and 6(b)], 45 s [Figures 6(c) and 6(d)], 35 s [Figures 6(e) and 6(f)]; signal-to-noise ratio: 0.6 [Figures 6(a) and 6(b)], 0.38 [Figures 6(c) and 6(d)], 0.31 [Figures 6(e) and 6(f)].

also be increased by increasing the signal values, i.e., increasing the recording time of one diffraction pattern. In order to “pull out” several reflections of low intensity for each of several crystalline phases, it will take time, calculated in tens of hours of diffractometer operation, which in most cases is unacceptable.

The identification of weak reflections of crystalline phases with intensity less than the noise component of the background was achieved due to the use of the permutation test in the X-ray diffraction data processing method. We know about the use of the permutation test in the processing of X-ray diffraction data by French specialists (Paradis-Fortin et al., 2022) in 2022. We used a permutation test to detect weak reflections earlier in 2019 (Skorbun et al., 2019) in an article on our method for processing X-ray diffraction data for multiphase materials with a low content of phases.

To increase the background values, both the average values of the background intensity  $\langle I_b \rangle$  and the values of the “noise” component of the background  $\Delta I_b$ , we used  $\gamma$ -quanta emitted by a sample of LFCM. Our series of experiments indicate that the following components contributed to the background recorded on the diffractometer: the background of the diffractometer registration system (instrument background),  $\gamma$ -quanta obtained as a result of beam scattering on a sample of  $\alpha$ -quartz and  $\gamma$ -quanta emitted by a sample of lava-like fuel-containing material.

Analysis of the data in Tables II–IV shows that the average values of the background intensity  $\langle I_b \rangle$  (Table IV, column 4, counting time 195 s) consist of 48% from  $\gamma$ -quanta recorded by the diffractometer registration system, 18% from  $\gamma$ -quanta scattered on  $\alpha$ -quartz and 34% of  $\gamma$ -quanta emitted by a sample of lava-like fuel-containing material. The data in these tables also show that the “noise” component of the background ( $\Delta I_b$ ) (Table IV, column 6, counting time 195 s) consists of 80%  $\gamma$ -quanta recorded by the diffractometer registration system and 20%  $\gamma$ -quanta emitted by a sample of lava-like fuel-containing material. There is no contribution from  $\gamma$ -quanta scattered by the  $\alpha$ -quartz sample.

The results indicate that our method of processing X-ray diffraction data makes it possible to detect quartz reflections from the “noise” component of the background at the signal-to-noise ratio of more than 0.2. It should be noted that at the signal-to-noise ratio in the range of 0.4–0.2, the method of processing X-ray diffraction data gives less reliability. The reliability of the presence of reflections is low.

## V. CONCLUSION

1. Method of processing X-ray diffraction data makes it possible to reliably separate the reflections of crystalline phases at the signal-to-noise ratio of more than 0.4. With a decrease in this ratio to 0.2, the above method demonstrates less reliability, and the data obtained require a more detailed analysis. The method demonstrates practically unacceptable reliability at the signal-to-noise ratio of less than 0.2, and the obtained data require confirmation.
2. The X-ray diffraction data processing method makes it possible to increase the possibilities of the X-ray phase analysis method due to the selection of reflections of crystalline phases, which are “hidden” in the noise of diffraction patterns. Using these two methods makes it possible to identify crystalline

phases with a low (down to 0.1 wt.%) content. For most studied materials phases with such content are secondary, since they are caused by additives and inevitable impurities in the material (or in the original components from which the material under study is obtained). The possibility of identifying and evaluating the content of such phases will allow material developers to find out their role and degree of influence on the microstructure of the material under study and, accordingly, opens up opportunities for improving the physicochemical properties of materials.

## ACKNOWLEDGEMENTS

The work was sponsored in the framework of the budget theme of the National Academy of Sciences of Ukraine (No. 0120U103480).

## CONFLICT OF INTEREST

The authors declare no conflicts of interest.

## REFERENCES

- Duée, C., B. Orberger, N. Maubec, V. Laperche, L. Capar, A. Bourguignon, X. Bourrat, Y. El Mendili, D. Chateigner, S. Gascoin, M. Le Guen, C. Rodriguez, F. Trotet, M. Kadar, K. Devaux, M. Ollier, H. Pillière, T. Lefèvre, D. Harang, F. Eijkelkamp, H. Nolte, and P. Koert. 2019. “Impact of Heterogeneities and Surface Roughness on pXRF, pIR, XRD and Raman Analyses: Challenges for On-Line, Real-Time Combined Mineralogical and Chemical Analyses on Drill Cores and Implication for “High Speed” Ni-Laterite Exploration.” *Journal of Geochemical Exploration* 198: 1–17. doi:10.1016/j.gexplo.2018.12.010.
- Gabielkov, S. V., I. V. Zhyganiuk, V. V. Dolin, A. D. Skorbun, V. G. Kudlai, P. E. Parkhomchuk, V. M. Slyvinsky, and S. O. Chikolovets. 2023. “Phase Composition of Lava-Like Fuel-Containing Materials of Unit 4 of the Chernobyl NPP. Black Ceramics.” *Journal of Nuclear Materials* 579: 154392. doi:10.1016/j.jnucmat.2023.154392.
- Garin, J. L., and R. L. Mannheim. 2012. “Rietveld Quantitative Analysis of Cast Super Duplex Steel.” *Powder Diffraction* 27 (2): 131–5. doi:10.1017/s0885715612000383.
- Guinebretière, R. 2007. *X-Ray Diffraction by Polycrystalline Materials*. New York, Wiley.
- Kroll, P., and M. Milko. 2003. “Theoretical Investigation of the Solid State Reaction of Silicon Nitride and Silicon Dioxide Forming Silicon Oxynitride ( $\text{Si}_2\text{N}_2\text{O}$ ) Under Pressure.” *Zeitschrift Fur Anorganische Und Allgemeine Chemie* 629 (10): 1737–50. doi:10.1002/zaac.200300122.
- Loy, C. W., K. A. Matori, N. Zainuddin, A. E. Whitten, C. Rehm, L. de Campo, A. Sokolova, and S. Schmid. 2017. “Crystallographic Characterization of Fluorapatite Glass-Ceramics Synthesized from Industrial Waste.” *Powder Diffraction* 32: S61–5. doi:10.1017/s088571561700094x.
- Machatschki, F. 1936. “Die Kristallstruktur von Tiefquarz  $\text{SiO}_2$  und Aluminiumorthoarsenat  $\text{AlAsO}_4$ .” *Zeitschrift für Kristallographie – Crystalline Materials* 94: 222–30. doi:10.1524/zkri.1936.94.1.222.
- Madsen, I. C., and R. J. Hill. 1994. “Collection and Analysis of Powder Diffraction Data with Near-Constant Counting Statistics.” *Journal of Applied Crystallography* 27: 385–92. doi:10.1107/s0021889893008593.
- Moore, D. S., G. P. McCabe, and B. A. Craig. 2014. *Introduction to the Practice of Statistics*. New York, W. H. Freeman and Company.
- Murugesan, G., K. R. Nandhan, N. Maruthi, A. Muthuraja, S. Bhaskar, and M. Manigandan. 2023. “Structural Analysis of  $\text{Ba}_{0.8}\text{Sr}_{0.2}\text{Ti}_{0.6}\text{Zr}_{0.3}\text{Mn}_{0.1}\text{O}_3$  Ceramics.” *Powder Diffraction* 38 (1): 27–9. doi:10.1017/s0885715622000598.
- Paradis-Fortin, L., P. Lemoine, E. Guilmeau, B. Malaman, E. Elkaim, A. Zitolo, S. Cordier, G. Guelou, B. Raveau, and C. Prestipino. 2022. “Resolution of the Cationic Distribution in Synthetic Germanite  $\text{Cu}_{22}\text{Fe}_8\text{Ge}_4\text{S}_{32}$  by an Experimental Combinatorial Approach Based on Synchrotron Resonant Powder Diffraction Data: A Case Study and

- Guidelines for Analogous Compounds.” *Chemistry of Materials* 34 (16): 7434–45. doi:10.1021/acs.chemmater.2c01561.
- Putz, H. 2023. Match! - Phase Analysis using Powder Diffraction, Version 3.16. (Computer Software) Crystal Impact, Kreuzherrenstr. 102, 53227 Bonn, Gemany.
- Sariel, J., I. Dahan, and Y. Gelbstein. 2008. “Rhombohedral-Cubic Phase Transition Characterization of (Pb,Ge)Te Using High-Temperature XRD.” *Powder Diffraction* 23 (2): 137–40. doi:10.1154/1.2912439.
- Skorbun, A. D., S. V. Gabielkov, I. V. Zhyganiuk, V. G. Kudlai, P. E. Parkhomchuk, and S. A. Chikolovets. 2019. “Method of X-Ray Diffraction Data Processing for Multiphase Materials with Low Phase Contents.” *Ukrainian Journal of Physics* 64 (9): 870–8.
- Taguchi, T., C. Bronnimann, and E. F. Eikenberry. 2008. “Next Generation X-Ray Detectors for In-House XRD.” *Powder Diffraction* 23 (2): 101–5. doi:10.1154/1.2912455.
- Wiessner, M., P. Angerer, S. van der Zwaag, and E. Gamsjager. 2021. “Transient Phase Fraction and Dislocation Density Estimation From In-Situ X-ray Diffraction Data with a Low Signal-to-Noise Ratio Using a Bayesian Approach to the Rietveld Analysis.” *Materials Characterization* 172: 110860. doi:10.1016/j.matchar.2020.110860.
- Wilkins, M. C. D., M. C. Stennett, and N. C. Hyatt. 2020. “The Effect of A-Site Cation on the Formation of Brannerite (ATi(2)O(6), A = U, Th, Ce) Ceramic Phases in a Glass-Ceramic Composite System.” *Mrs Advances* 5 (1–2): 73–81. doi:10.1557/adv.2019.470.